Cell Reports

Anabolism-Associated Mitochondrial Stasis Driving Lymphocyte Differentiation over Self-Renewal

Graphical Abstract

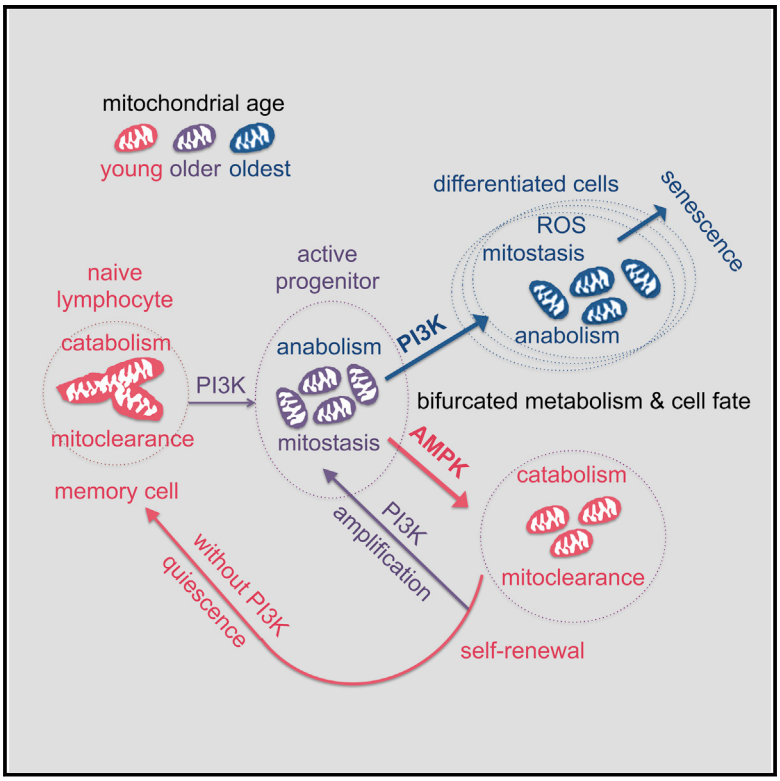

Highlights

- Activated lymphocytes yield sibling cells with unequal clearance of aged mitochondria
- Stasis of progenitor mitochondria marks T cells destined for differentiation in vivo
- Mitochondrial stasis is linked to anabolism, inhibited autophagy, and glycolysis
- Key transcription factors intertwine the control of metabolic program and cell fate

Authors

William C. Adams, Yen-Hua Chen, Radomir Kratchmarov, ..., Jeffrey C. Rathmell, Hans-Willem Snoeck, Steven L. Reiner

Correspondence

sr2978@cumc.columbia.edu

In Brief

Activated lymphocytes use asymmetric cell division to couple differentiation and self-renewal. Adams et al. show that unequal elimination of aged mitochondria by sibling cells is part of a broader dichotomy of metabolic signaling, which instructs cells to use nutrients for division and differentiation or instead to catabolically self-digest for self-renewal.

Adams et al., 2016, Cell Reports *17*, 3142–3152
December 20, 2016
http://dx.doi.org/10.1016/j.celrep.2016.11.065

CellPress

OPEN ACCESS
CellPress

Cell Reports
Report

Anabolism-Associated Mitochondrial Stasis Driving Lymphocyte Differentiation over Self-Renewal

William C. Adams,[1,6] Yen-Hua Chen,[1,6] Radomir Kratchmarov,[1,6] Bonnie Yen,[1] Simone A. Nish,[1] Wen-Hsuan W. Lin,[1] Nyanza J. Rothman,[1] Larry L. Luchsinger,[2] Ulf Klein,[3] Meinrad Busslinger,[4] Jeffrey C. Rathmell,[5] Hans-Willem Snoeck,[2] and Steven L. Reiner[1,7,*]

[1]Department of Microbiology and Immunology and Department of Pediatrics, Columbia University Medical Center, New York, NY 10032, USA
[2]Department of Medicine and Department of Microbiology and Immunology, Columbia University Medical Center, New York, NY 10032, USA
[3]Department of Pathology and Department of Microbiology and Immunology, Columbia University Medical Center, New York, NY 10032, USA
[4]Research Institute of Molecular Pathology, Vienna Biocenter, 1030 Vienna, Austria
[5]Vanderbilt Centre for Immunobiology, Department of Pathology, Microbiology, and Immunology, Vanderbilt University Medical Center, Nashville, TN 37232, USA
[6]Co-first author
[7]Lead Contact
*Correspondence: sr2978@cumc.columbia.edu
http://dx.doi.org/10.1016/j.celrep.2016.11.065

SUMMARY

Regeneration requires related cells to diverge in fate. We show that activated lymphocytes yield sibling cells with unequal elimination of aged mitochondria. Disparate mitochondrial clearance impacts cell fate and reflects larger constellations of opposing metabolic states. Differentiation driven by an anabolic constellation of PI3K/mTOR activation, aerobic glycolysis, inhibited autophagy, mitochondrial stasis, and ROS production is balanced with self-renewal maintained by a catabolic constellation of AMPK activation, mitochondrial elimination, oxidative metabolism, and maintenance of FoxO1 activity. Perturbations up and down the metabolic pathways shift the balance of nutritive constellations and cell fate owing to self-reinforcement and reciprocal inhibition between anabolism and catabolism. Cell fate and metabolic state are linked by transcriptional regulators, such as IRF4 and FoxO1, with dual roles in lineage and metabolic choice. Instructing some cells to utilize nutrients for anabolism and differentiation while other cells catabolically self-digest and self-renew may enable growth and repair in metazoa.

INTRODUCTION

Clonal selection of B and T lymphocytes during an immune response requires an activated progenitor cell to produce differentiated functional descendants, marked by PI3K-driven silencing of the developmentally critical transcription factors Pax5 and TCF1, respectively (Lin et al., 2015, 2016; Nish et al., 2017). Sibling cells of differentiated progeny, by contrast, appear to self-renew owing to unequal transmission of PI3K signaling. In view of the suggested importance of clearance of aged mitochondria in self-renewal (García-Prat et al., 2016; Ito et al., 2016; Katajisto et al., 2015; O'Sullivan et al., 2015), we examined the stasis and clearance of mitochondria in activated lymphocytes. We found that unequal elimination of aged mitochondria between differentiating and self-renewing lymphocytes was a reflection of a more global bifurcation of anabolic versus catabolic signaling, which is coupled to control of their divergent cell fate.

RESULTS

Clearance and Stasis of Aged Mitochondria Impact Lymphocyte Cell Fate

T cells undergoing TCF1 silencing during functional differentiation are incapable of reverting to TCF1 expression under physiological conditions in vivo and in vitro (Im et al., 2016; Lin et al., 2016; Nish et al., 2017; Utzschneider et al., 2016). Plasma cell differentiation during immunization and modeled differentiation is characterized by a bifurcation of self-renewing $Pax5^{hi}$ B cells and differentiated $Pax5^{lo}$ plasma cells (Figure S1A; Lin et al., 2015; Shi et al., 2015; Xu et al., 2015). We tested whether PI3K-driven differentiation in vitro using lipopolysaccharide (LPS) (Keppler et al., 2015) causes irreversible commitment to Pax5 silencing. Stimulation of splenic B cells mirrors the response of purified naive follicular B cells, with $Pax5^{lo}$ cells arising after several divisions (Figure S1B). Using cells from Pax5-IRES-human CD2 reporter mice (Fuxa and Busslinger, 2007), we sorted $Pax5(hCD2)^{hi}$ and $Pax5(hCD2)^{lo}$ cells from later cell generations of splenic B cells activated by LPS and re-plated them in fresh media containing LPS. $Pax5^{lo}$ cells were incapable of reverting to Pax5 expression, whereas $Pax5^{hi}$ cells remained bi-potent, capable of producing $Pax5^{lo}$ progeny and self-renewing the $Pax5^{hi}$ lineage (Figure 1A). Like TCF1 silencing in T cells (Lin et al., 2016), silencing of Pax5 required cell cycle progression (Figure S1C).

Using genetic and pharmacological approaches to interfere with Dynamin-related protein 1 (Drp1), which is essential for mitochondrial fission and autophagy (Mishra and Chan, 2014), we began testing the role of mitochondrial clearance in lymphocyte fate. Transduction of activated B and T cells with dominant-negative (DN) Drp1 retroviral vector (Frank et al., 2001) or the

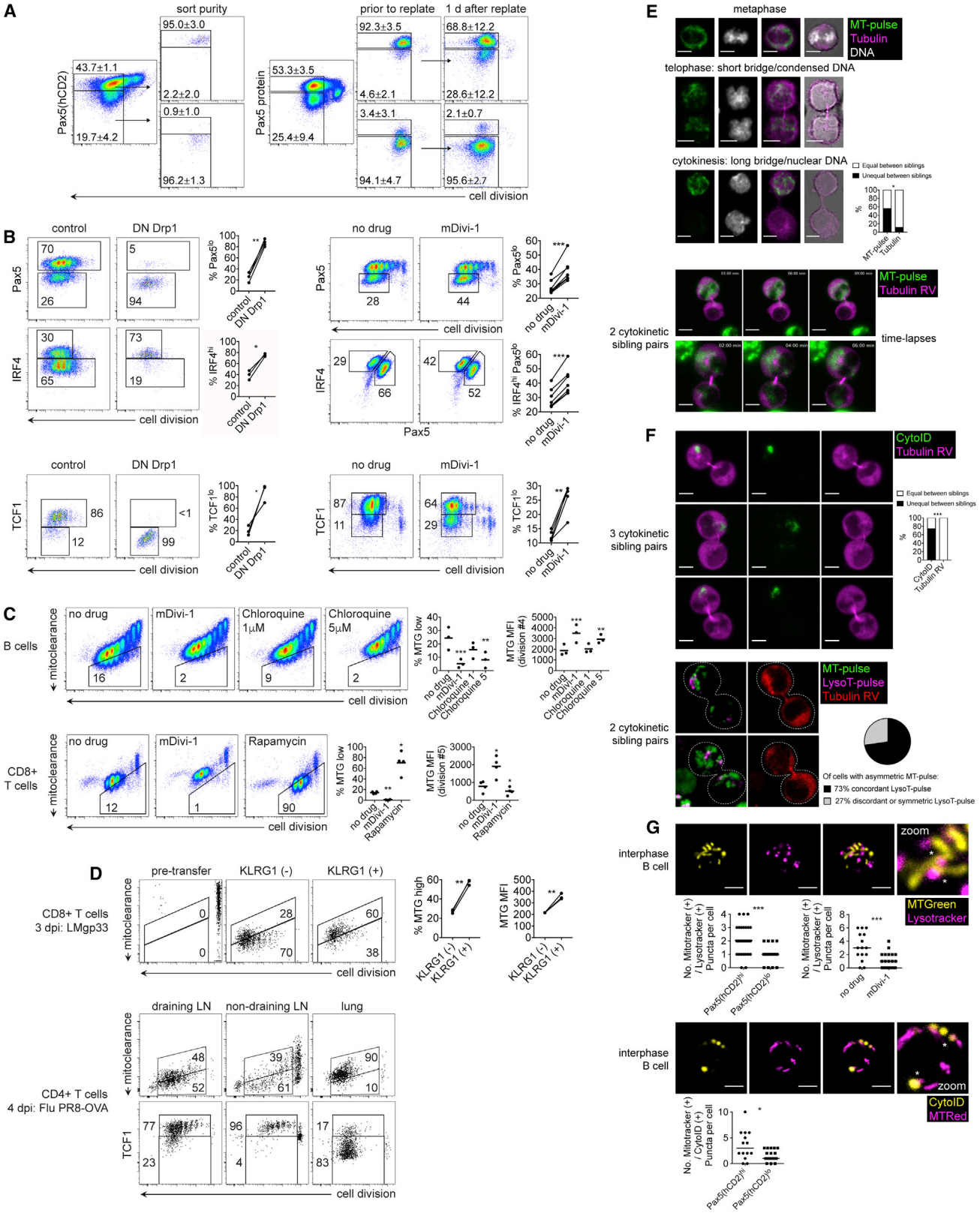

(legend on next page)

pharmacological inhibitor of Drp1, mDivi-1, led to enhanced plasmablast and effector T cell differentiation, as measured by more frequent repression of Pax5 and TCF1, respectively (Figure 1B). In addition, DN Drp1 and mDivi-1 caused reciprocal elevation in IRF4 abundance in B cells (Figure 1B), a characteristic of committed plasmablasts (Figure S1A; Lin et al., 2015; Xu et al., 2015).

We used flow cytometry to monitor clearance of aged mitochondria in relation to cell division number (Figure S1D). Prior to activation, lymphocytes were pulsed with both a fluorescent mitochondrial dye (Chazotte, 2011) and a fluorescent dye that labels cellular proteins and allows determination of division number (Quah and Parish, 2012). Following activation, dilution of the division dye (x axis leftward progression) and clearance (sum of passive dilution plus active destruction) of mitochondrial dye (y axis downward progression) could be monitored with flow cytometry (Figures 1C and S1D). Treatment with mDivi-1 increased stasis of aged (pulsed) mitochondria comparably to treatment with an

Figure 1. Clearance and Stasis of Aged Mitochondria Impact Lymphocyte Cell Fate

(A) Left plots: LPS-activated, Pax5(hCD2) reporter B cells were sorted from later cell generations based on hCD2 expression, and post-sort purity of live cells is shown. Right plots: pre-sort Pax5 protein staining of fixed cells next to Pax5 protein staining of sorted cells, followed by Pax5 protein staining of sorted populations 1 day after re-plating in fresh media containing LPS are shown. Plots depict one representative experiment and numbers are summary statistics (mean ± SD, n = 5) for frequency of cells in the corresponding gate.

(B) Top left panel: cell division versus Pax5 and IRF4 expression of naive B cells stimulated in vitro with LPS. At 36 hr after stimulation, cells were transduced with control retrovirus (RV) or RV encoding dominant-negative (DN) Drp1 and returned to stimulatory conditions for 36 hr. Only transduced cells are shown. Horizontal numbers denote the frequency of cells within a bound area (i.e., gate). Adjacent graphs denote the frequency of $Pax5^{lo}$ (n = 4; $^{**}p < 0.01$, two-tailed paired t test) and $IRF4^{hi}$ (n = 3; $^{*}p < 0.05$, two-tailed paired t test) cells among B cells transduced with control or DN Drp1 RV. DN Drp1 RV increased the frequency of $Pax5^{lo}$ cells from 25.3 ± 7.6 to 86.9 ± 6.1 and $IRF4^{hi}$ cells from 39.2 ± 8.5 to 75.5 ± 2.6 compared to control RV (mean ± SD). Lower left panel: CTV-labeled $CD8^+$ T cells were stimulated with anti-CD3 and anti-CD28 antibodies with IL-2 for 36 hr, then transduced with control or DN Drp1 RV, and analyzed by fluorescence-activated cell sorting (FACS) for cell division versus TCF1 expression 36 hr after transduction. Only transduced cells are shown. Graph indicates the frequency of $TCF1^{lo}$ T cells among cells transduced with control or DN Drp1 RV (n = 3; $^{*}p < 0.05$, two-tailed paired t test). DN Drp1 RV increased the frequency of $TCF1^{lo}$ cells from 20.1 ± 8.6 to 88.4 ± 16.2 compared to control RV (mean ± SD). Top right panel: CTV-labeled B cells from wild-type mice were stimulated with LPS in the absence or presence of mDivi-1 (10 μM) inhibitor of Drp1 for 66 hr. Graphs indicate the frequency of $Pax5^{lo}$ and $Pax5^{lo}IRF4^{hi}$ B cells among cells activated in the absence or presence of mDivi-1 (n = 7; $^{***}p < 0.005$, two-tailed paired t test). mDivi-1 increased the frequency of $Pax5^{lo}$ cells from 27.8 ± 4.9 to 39.41 ± 8.5 and $Pax5^{lo}IRF4^{hi}$ cells from 29.5 ± 6.9 to 41.3 ± 9.5 compared to no drug treatment (mean ± SD). Lower right panel: CTV-labeled P14 transgenic $CD8^+$ T cells were stimulated with gp33-41 and IL-2 for 4 days in the absence or presence of mDivi-1 (10 μM). Graph indicates the frequency of $TCF1^{lo}$ T cells among cells activated in the absence or presence of mDivi-1 (n = 5; $^{**}p < 0.01$, two-tailed paired t test). mDivi-1 increased the frequency of $TCF1^{lo}$ cells from 12.5 ± 1.8 to 26.0 ± 5.1 (mean ± SD) compared to no drug.

(C) FACS of CTV-labeled and MitoTracker Green FM (MTG)-pulsed activated B cells (top row) and P14 $CD8^+$ T cells (bottom row) stimulated with LPS or gp33-41 peptide and IL-2, respectively, for 66 hr. Cells were cultured in the absence or presence of mDivi-1 (10 μM), Chloroquine (1 and 5 μM, left to right), or rapamycin (1 nM) as indicated. Reverse arrow on the y axis indicates dilution plus elimination of pre-labeled (pulsed) mitochondria, termed mitoclearance, in relation to cell division (x axis). Upper row statistics are the frequency of cells within the entire trapezoidal MTG low gate (left) and mean fluorescence intensity (MFI) of MTG signal in the fourth cell division (right) (n = 3; $^{**}p < 0.01$ and $^{***}p < 0.005$ for indicated treated groups compared to no drug control group, repeated-measures one-way ANOVA). Lower row graphs are the frequency of cells within entire trapezoidal MTG low gate (left) and MFI of MTG signal in the fifth cell division (right) (n = 3; $^{*}p < 0.05$ or $^{**}p < 0.01$ for treated versus control group, repeated-measures one-way ANOVA).

(D) CTV and MTG pulse-labeled P14 $CD8^+$ T cells (top row) and OT-II $CD4^+$ T cells (bottom panels) were adoptively transferred into congenically disparate recipients challenged with Listeria (LMgp33) or PR8-OVA influenza virus, respectively. For $CD8^+$ T cells, the left plot depicts cell division versus mitoclearance for non-transferred cells as a control for starting fluorescence of MTG pulse labeling. Middle and right plots represent $KLRG1^-$ and $KLRG1^+$ (known to be $TCF1^{lo}$ [Lin et al., 2015, 2016]) CD8+ donor T cells from recipient mice 3 days post Listeria challenge. Statistics denote the frequency of MTG high cells (left) and the MTG MFI of all cells in the indicated $KLRG1^-$ and $KLRG1^+$ groups (right) (n = 3; $^{**}p < 0.01$, two-tailed paired t test). For $CD4^+$ T cells, the upper row depicts cell division versus mitoclearance in draining lymph nodes (LNs), non-draining LNs, and lung tissue; the bottom row depicts cell division versus TCF1 expression. Numbers are the frequency within gates encompassing divided cells. $CD4^+$ FACS plots are representative of two identical experiments.

(E) Top panels: MitoTracker Red FM (MTR)-pulsed, LPS-stimulated B cells fixed after 44 hr and stained with DNA dye and anti-tubulin antibodies. One representative metaphase (symmetric), telophase (symmetric), and cytokinetic (asymmetric) event is shown. The experiment was repeated three times (metaphase, n = 11 cells; telophase, n = 8 sibling pairs; and cytokinesis, n = 18 sibling pairs). The graph depicts the percentage of sibling cell pairs with equal or unequal ratios of MTR and tubulin ($^{*}p < 0.05$, Fisher's exact test). Bottom panels: two representative time-lapse series of LPS-stimulated B cells transduced with mCherry-alpha-tubulin RV and pulsed with MTG 16 hr prior to imaging are shown. Frames, left to right, represent 3-min (upper row) and 2-min (lower row) intervals (n = 3). Scale bars, 5 μm.

(F) Confocal images of live, LPS-stimulated B cells transduced with mCherry-alpha-tubulin RV and labeled with CYTO-ID. Top panel: three representative cytokinetic sibling pairs are shown (n = 19 sibling pairs, 74% asymmetric; $^{***}p < 0.005$, Fisher's exact test). Bottom panel: confocal images show live, LPS-stimulated B cells transduced with mCherry-alpha-tubulin RV and co-pulsed with MTG and LysoTracker 16 hr prior to imaging. Of the cells imaged, 73% had concordant asymmetric MTG and LysoTracker abundance (n = 11 sibling pairs). Scale bars, 5 μm.

(G) LPS-activated, Pax5(hCD2) reporter B cells 3 days post-stimulation were sorted from later cell generations based on surface hCD2 expression, as in (A). Cells were then labeled with MTG and LysoTracker DeepRed (top panels show representative image) or CYTO-ID and MTR (bottom panels show representative image). Steady-state mitophagy was determined by co-localization of individual mitochondrial puncta with LysoTracker or CYTO-ID puncta. Top left graph indicates the number of co-localized MTG/LysoTracker DeepRed puncta among $Pax5^{hi}$ (n = 35) and $Pax5^{lo}$ (n = 17) cells, with a mean of two puncta and one punctum, respectively ($^{***}p < 0.005$, Mann-Whitney test). Top right graph indicates the number of co-localized MTG/LysoTracker DeepRed puncta, among $Pax5(hCD2)^{hi}$ cells sorted from cultures stimulated in the absence (n = 15) or presence (n = 21) of mDivi-1, with a mean of three puncta and one punctum, respectively ($^{***}p < 0.005$, Mann-Whitney test). Bottom graph indicates the number of co-localized MTR/CYTO-ID puncta among $Pax5^{hi}$ (n = 14) and $Pax5^{lo}$ (n = 19) cells, with a mean of three puncta and one punctum, respectively ($^{*}p < 0.05$, Mann-Whitney test). Scale bars, 5 μm. The fourth panel in each row is a zoomed-in version of the third panel.

See also Figure S1.

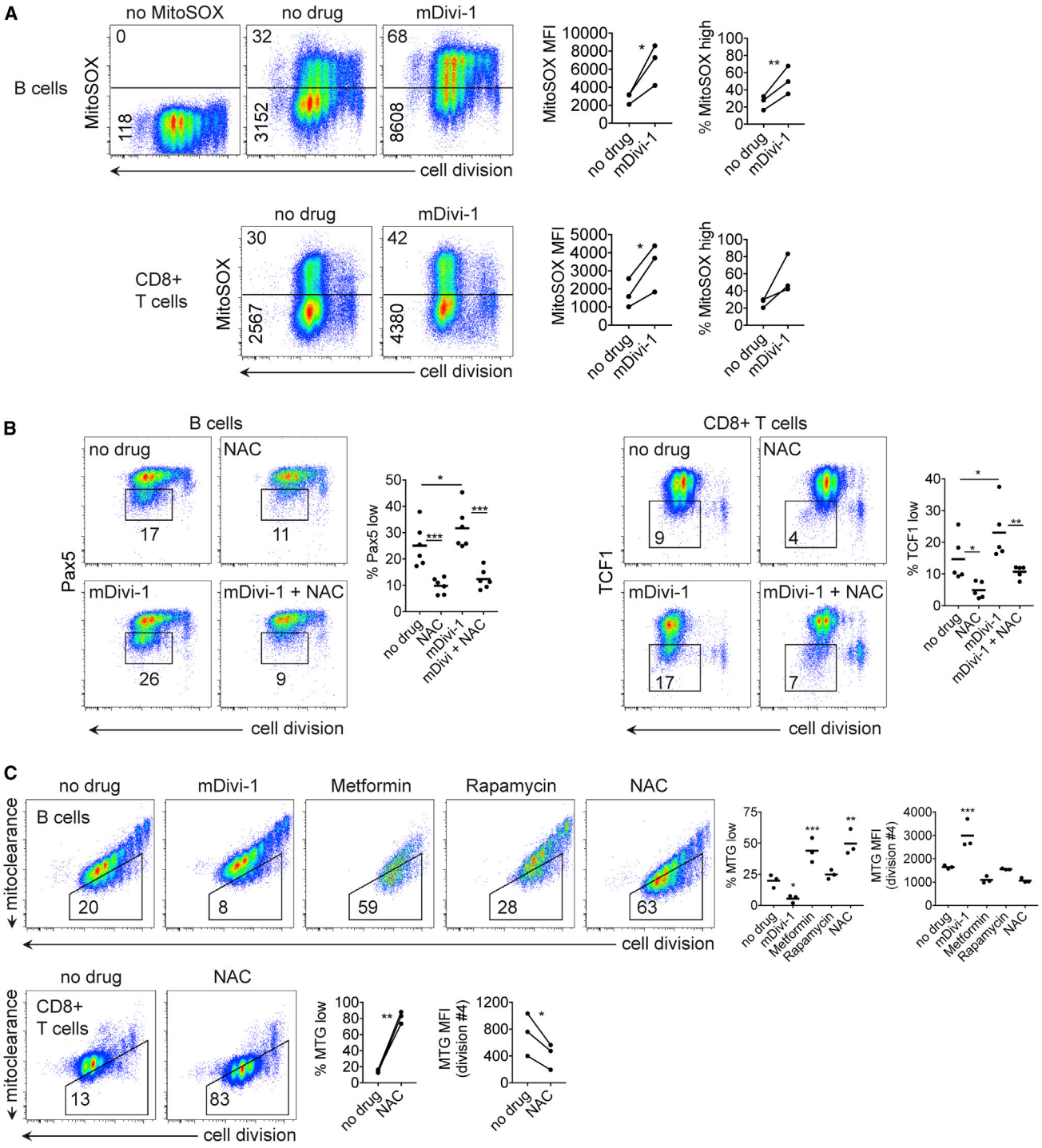

Figure 2. ROS Mediate the Effects of, and Reinforce the Stasis of, Aged Mitochondria

(A) CTV-labeled B cells (upper row) and P14 CD8+ T cells (lower row) stimulated with LPS or gp33-41 peptide and IL-2, respectively, in the absence or presence of mDivi-1 (10 μM) and analyzed on day 3 for cell division versus mitochondrial ROS (MitoSOX). Horizontal numbers denote the frequency of cells within gate. Vertical numbers denote MFI of all cells, not simply those within gate. Upper graphs display MitoSOX MFI (left) and the frequency of MitoSOX^{hi} cells (right) among B cells stimulated in the absence or presence of mDivi-1 (n = 3; *p < 0.05 or **p < 0.01, two-tailed paired t test). Lower graphs display MitoSOX MFI (left) and the frequency of MitoSOX^{hi} cells (right) among T cells stimulated in the absence or presence of mDivi-1 (n = 3; *p < 0.05, two-tailed paired t test).

(B) B cells stimulated with LPS (left panels) or P14 CD8^{+} T cells stimulated with gp33-41 peptide and IL-2 (right panels) in the absence or presence of mDivi-1 (10 μM), without or with the addition of NAC (3 mM for B cells and 5 mM for T cells) and analyzed for Pax5 or TCF1 expression. Left graph displays the frequency of

(legend continued on next page)

inhibitor of general macro-autophagy (chloroquine) and in contrast to treatment with a stimulant of general macro-autophagy (rapamycin), which increased clearance (Figure 1C).

Because inheritance of some parent cell mitochondria was evident for at least six cell generations (Figures 1C and S1D), we examined T cells undergoing differentiation in vivo. At 3 days following *Listeria* infection, terminally differentiated $CD8^+$ $KLRG1^+$ T cells, a subset of effector-determined $TCF1^{lo}$ cells (Lin et al., 2015, 2016), were enriched with high levels of aged mitochondria (Figure 1D). At 4 days following respiratory infection with influenza virus, $CD4^+$ Th1 effector cells (largely $TCF1^{lo}$) left the draining lymph node to populate the lung, while self-renewing $TCF1^{hi}$ central memory cells left the draining lymph node to recirculate through non-draining nodes (Nish et al., 2017). Lung-resident effector cells were enriched with the stasis of aged mitochondria (Figure 1D). Self-renewing, non-draining lymph node $CD4^+$ T cells were reciprocally enriched with the clearance of aged mitochondria (Figure 1D). Cellular progeny that are destined for differentiation in vivo are thus marked by the stasis of aged mitochondria.

Using confocal microscopy, we found that subcellular distribution of aged (pulsed) mitochondria was generally symmetric in metaphase and early telophase cells (Figure 1E). In cytokinesis, however, we found that the abundance of aged mitochondria between sibling pairs was frequently discordant (Figure 1E). Autophagosome abundance was also unequal in cytokinetic, conjoined sibling cells (Figure 1F), and the clearance of aged (pulsed) mitochondria was coordinate with the clearance of aged (pulsed) lysosomes (Figure 1F). To determine whether mitochondrial digestion correlated with cell fate, we sorted self-renewing $Pax5(hCD2)^{hi}$ and differentiated $Pax5(hCD2)^{lo}$ singlet cells from the same range of later cell generations, and then we stained mitochondria together with either lysosomes or autophagic organelles. Co-localization of mitochondrial puncta with lysosomal or autophagic puncta occurred at increased incidence in self-renewing $Pax5^{hi}$ cells (Figure 1G). In addition, mDivi-1 treatment, which reduces mitoclearance by flow cytometry (Figure 1C), decreased the steady-state incidence of co-localized mitochondrial and lysosomal puncta in $Pax5^{hi}$ cells (Figure 1G). Together these findings suggest that the stasis of aged mitochondria characterizes and drives functional differentiation of T and B cells.

Reactive Oxygen Mediates the Effects of, and Reinforces the Stasis of, Aged Mitochondria

Impaired self-renewal resulting from the stasis of aged mitochondria can be mediated by elevated reactive oxygen species (ROS) (García-Prat et al., 2016; O'Sullivan et al., 2015). We found mitochondrial and cellular ROS increased after mDivi-1 treatment (Figures 2A and S2A). Scavenging ROS with N-Acetyl-L-cysteine (NAC) promoted self-renewal (less frequent repression of Pax5 and TCF1) under normal stimulatory conditions and suppressed the over-differentiation phenotype of mDivi-1 treatment and DN Drp1 expression (Figures 2B and S2B). Consistent with a model wherein ROS promotes differentiation, cells with higher mitochondrial ROS content were enriched with greater stasis of aged mitochondria (Figure S2C). Unexpectedly, we found that ROS not only mediate the effects of mitochondrial stasis but also perpetuate mitochondrial stasis. Scavenging ROS stimulated the clearance of aged mitochondria (Figure 2C) in a manner mimicking other stimulants of general macro-autophagy (Figures 1C and 2C).

Aerobic Glycolysis Linking an Anabolic Constellation to Differentiation

The self-reinforcing relationship between mitochondrial stasis and ROS prompted us to test the effects of metabolism on lymphocyte differentiation. Both B and T cells utilize aerobic glycolysis during activation and differentiation (Caro-Maldonado et al., 2014; Chang et al., 2013; Frauwirth et al., 2002; Sukumar et al., 2013). Treatment with 2-Deoxy-D-glucose (2-DG), to inhibit glycolytic flux, shifted the balance of lymphocyte fate toward self-renewal under normal stimulatory conditions (Figure 3A). 2-DG treatment also suppressed the over-differentiation phenotype of mDivi-1 treatment (Figure 3A). In contrast, stimulation of glycolytic flux by retroviral overexpression of the rate-limiting enzyme hexokinase 2 (Roberts and Miyamoto, 2015) resulted in an over-differentiation phenotype with more cells undergoing Pax5 and TCF1 repression, respectively (Figure 3B). Preventing aerobic glycolysis by substituting galactose for glucose also skewed cell fate toward self-renewal, while inhibiting oxidative phosphorylation with oligomycin stimulated greater differentiation (Figure S3A). Inhibiting glycolytic flux also increased the clearance of aged mitochondria, augmented general macro-autophagy, reduced cellular ROS content, and suppressed mTOR activation (Figures 3C and S3B).

Anabolic versus Catabolic Bistability Balancing Differentiation and Renewal

The foregoing results suggest that anabolism associated with aerobic glycolysis, mitochondrial stasis, inhibited autophagy, and elevated ROS content is in a positive feedback loop that reinforces anabolic signal transduction for continued nutrient uptake and utilization. We, therefore, assessed the relationship between anabolic and catabolic signaling in activated lymphocytes. Deprivation of glucose led to rapid downregulation of anabolism-associated mTOR activation (phospho-S6) and reciprocal induction of catabolism-associated AMPK activation (as indicated by an increase in phospho-Acetyl-CoA Carboxylase) (Figures 4A

$Pax5^{lo}$ B cells in groups stimulated under the indicated conditions (n = 6; $^*p < 0.05$ or $^{***}p < 0.005$, repeated-measures one-way ANOVA). Right graph displays the frequency of $TCF1^{lo}$ cells in groups stimulated under the indicated conditions (n = 5; $^*p < 0.05$ or $^{**}p < 0.01$, repeated-measures one-way ANOVA).

(C) CTV-labeled, MTG-pulsed B cells stimulated with LPS (top panels) or P14 $CD8^+$ T cells stimulated with gp33-41 peptide and IL-2 (bottom panels) in the absence or presence of mDivi-1 (10 μM), metformin (300 nM), rapamycin (1 nM), or NAC (5 mM for B cells and 7 mM for T cells) analyzed for cell division versus mitoclearance on day 3. Data are representative of two experiments for each cell type. Upper row statistics denote the frequency of B cells within the entire trapezoidal MTG low gate (left) and MFI of MTG signal in the fourth cell division (right) (n = 3; $^*p < 0.05$, $^{**}p < 0.01$, or $^{***}p < 0.005$ for drug-treated groups compared to no drug control group, repeated-measures one-way ANOVA). Lower row statistics are the frequency of T cells within the entire trapezoidal MTG low gate (left) and MFI of MTG signal in the fourth cell division (right) (n = 3; $^*p < 0.05$ or $^{**}p < 0.01$, two-tailed paired t test).

See also Figure S2.

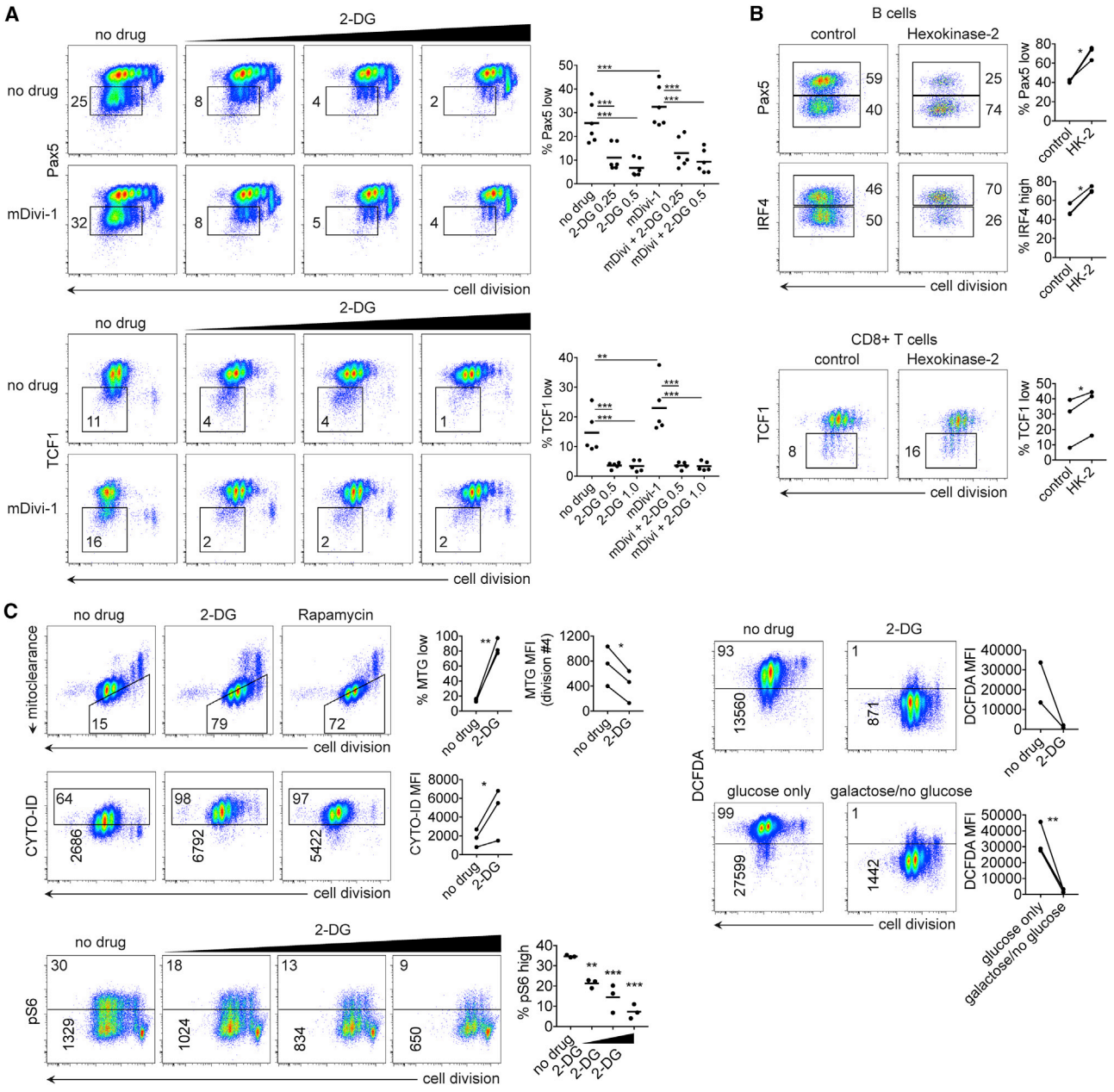

Figure 3. Aerobic Glycolysis Linking an Anabolic Constellation to Differentiation

(A) Top panels: cell division versus Pax5 expression of CTV-labeled B cells stimulated with LPS for 3 days in the absence or presence of mDivi-1 (10 μM) and increasing doses of 2-Deoxy-D-glucose (2-DG) (0, 0.25, 0.50, and 0.75 mM left to right). In these B cell experiments, drug variables were added 18 hr after stimulation. Bottom panels: cell division versus TCF1 expression of CTV-labeled P14 CD8$^+$ T cells stimulated for 4 days with gp33-41 peptide plus IL-2 in the absence or presence of mDivi-1 and increasing doses of 2-DG (0, 0.5, 1.0, and 2.0 mM), present from the beginning of stimulation, is shown. Upper statistical graph depicts the frequency of Pax5^{lo} B cells in the indicated conditions (n = 6; ***p < 0.005, repeated-measures one-way ANOVA). Lower statistical graph depicts the frequency of TCF1^{lo} CD8$^+$ T cells in the indicated conditions (n = 5; **p < 0.01 or ***p < 0.005, repeated-measures one-way ANOVA).

(B) Top panels: CTV-labeled B cells stimulated for 36 hr with LPS prior to transduction with control or hexokinase 2 (HK-2)-encoding RV and analyzed 36 hr after transduction for cell division versus Pax5 and IRF4. Only transduced events are shown. Statistics are the frequency of Pax5^{lo} (upper) and IRF4^{hi} (lower) cells among cells transduced with control or HK-2 RV (n = 3; *p < 0.05, two-tailed paired t test). Bottom panels: CTV-labeled CD8$^+$ T cells were stimulated with anti-CD3 and anti-CD28 antibodies with IL-2 for 36 hr prior to transduction with control RV or HK-2-encoding RV and analyzed 36 hr after transduction for cell division versus TCF1. Only transduced events are shown. The statistical graph depicts the frequency of TCF1^{lo} cells among cells transduced with control or HK-2 RV (n = 3; *p < 0.05, two-tailed paired t test).

(C) Upper left row: cell division versus mitoclearance of P14 CD8$^+$ T cells stimulated for 3 days with gp33-41 peptide and IL-2 in the absence or presence of 2-DG (2.0 mM) or rapamycin (10 nM). Statistics contain the frequency of cells within the MTG low trapezoidal gate (left) and the mean MFI of MTG signal in the fourth cell

(legend continued on next page)

and S3B). We also found that PI3K signaling was essential for mTOR activation (Figure 4B) while AMPK signaling was actively suppressing anabolic signaling, as indicated by the augmentation of pS6 found in AMPKα1-deficient cells (Figure 4B). More downstream perturbations to the catabolic process, such as inhibiting Drp1 (Figure 4B), caused similar augmentation in anabolic activation, further underscoring the negative feedback of catabolism on anabolism.

The anabolic versus catabolic signaling pathways also were found to have opposing effects on cell fate. Inhibitors of anabolism-associated PI3K/AKT/mTOR limit lymphocyte differentiation under normal conditions (Lin et al., 2015) and suppress the mDivi-1 over-differentiation phenotype (Figure 4C), analogously to scavenging ROS (Figure 2B) and inhibiting glycolysis (Figure 3A). Rapamycin, 2-DG, and NAC each caused a reduction in cell size (Figure S4), consistent with roles of mTOR, glycolytic flux, and ROS in cellular protein synthesis and anabolism (Iritani and Eisenman, 1999; Rathmell et al., 2000). Conversely, the inhibition of catabolism-associated FoxO1 stimulated greater plasma cell differentiation (Lin et al., 2015) and added to or synergized with a defective self-renewal phenotype that arose from mDivi-1 treatment and AMPKα1 deficiency (Figure 4C), a finding compatible with the loss of memory in AMPKα1-deficient T cells (Rolf et al., 2013).

IRF4, an essential transcription factor for plasmablast differentiation (Klein et al., 2006; Xu et al., 2015), has emerged as a regulator of glycolytic anabolism in lymphocytes (Lin et al., 2015; Man et al., 2013). We found that IRF4-deficient B cells exhibit excessive catabolism (hyper-elimination of aged mitochondria and reduced cell size), defective anabolism (weaker mTOR activation and glucose uptake), and absent Pax5 repression (Figures 4D and S4). Together with prior findings that FoxO1, a key mediator of cellular and organismal catabolism, is an essential guardian of Pax5 and TCF1 gene expression and lymphocyte self-renewal (Figure 4C; Lin et al., 2015), the present results are compatible with a model wherein some key transcription factors evolved to have dual functions as regulators of both metabolic state and cell fate.

DISCUSSION

Mitochondrial quality control and dynamics have been linked to stem cell renewal, tissue remodeling, cellular metabolism, and healthy aging, although the unifying mechanisms underlying their importance are not fully understood (Mishra and Chan, 2014). Clearance of aged mitochondria promotes self-renewal of hematopoietic, muscle, breast, and natural killer cells (García-Prat et al., 2016; Ito et al., 2016; Katajisto et al., 2015; O'Sullivan et al., 2015). Mitochondrial biogenesis (Bengsch et al., 2016; Scharping et al., 2016) and fusion (Buck et al., 2016; Khacho et al., 2016; Luchsinger et al., 2016) also support self-renewal of hematopoietic, neural, and memory T cells. Mitochondrial clearance, biogenesis, and fusion seemingly facilitate cellular self-renewal by eliminating dysfunctional organelles, making new organelles, and fusing nascent mitochondria to optimize the efficiency of oxidative metabolism.

The present findings support a model wherein mitochondrial stasis is part of a larger anabolic constellation of PI3K/AKT/mTOR activation, IRF4 induction, aerobic glycolysis, inhibited autophagy, mitochondrial stasis, ROS production, and inactivation of FoxO1 leading to silencing of Pax5 or TCF1. Conversely, mitochondrial clearance appears to be part of a larger catabolic constellation of AMPK activation, autophagy, mitochondrial elimination, oxidative metabolism, maintenance of FoxO1 activity, and Pax5 or TCF1 expression. Metabolic signaling appears to be inherently bi-stable, with each side (anabolism versus catabolism) having positive feedback of itself and mutual inhibition of the other side (double-negative feedback). Further investigation will be needed to determine what cellular component(s) are unequal at metaphase that drive the disparate metabolic constellations and cell fates. Determining whether cells with particular fates can change their patterns of glycolytic or respiratory metabolism also could lead to novel strategies for truncating or prolonging immune responses.

EXPERIMENTAL PROCEDURES

Mice

All animal work was conducted in accordance with Institutional Animal Care and Use Guidelines of Columbia University. Mice were housed in specific-pathogen-free conditions. C57BL/6 mice, Pax5-IRES-hCD2 reporter mice (Fuxa and Busslinger, 2007), P14 T cell receptor (TCR) transgenic mice recognizing LCMV peptide gp33-41/Db, OTII mice expressing an I-Ab-restricted TCR specific for ovalbumin amino acids 323–339, AMPKα1-knockout mice (Jørgensen et al., 2004) (Prkaa1tm1Vio), and IRF4-knockout mice (Klein et al., 2006) have been described previously. Mice that were 8–12 weeks old were used for most experiments.

Lymphocyte Activation

Spleens from mice were isolated and processed using established protocols. B cells were enriched from spleens by magnetic bead negative selection with MACS B cell isolation kit (Miltenyi Biotec). B cells (5×10^5 cells per well in 48-well plate) were cultured in Iscove's (Corning Life Sciences) complete media, unless specified otherwise, with LPS (20 μγ/mL; InvivoGen) for up to 3 days. Enriched $CD8^+$ T cells were obtained from spleens by magnetic bead negative selection with MACS $CD8^+$ T cell isolation kit (Miltenyi Biotec). $CD8^+$ T cells

division (right); (n = 3; *p < 0.05 or **p < 0.01, two-tailed paired t test). Middle left row: cell division versus autophagy (CYTO-ID stain) of P14 CD8+ T cells stimulated for 3 days with gp33-41 peptide and IL-2 in the absence or presence of 2-DG (2.0 mM) or rapamycin (10 nM) prior to CYTO-ID staining is shown. Statistics are MFI of CYTO-ID signal for the indicated groups (n = 3; *p < 0.05, two-tailed paired t test). Right panels: cell division versus total cellular ROS production (DCFDA stain) of P14 CD8+ T cells stimulated for 4 days with gp33-41 peptide plus IL-2 in the absence or presence of 2-DG (2 mM) (upper row) or in glucose-free media replete with glucose (10 mM) versus galactose (10 mM) (lower row) is shown. MFI of DCFDA staining in cells stimulated in the absence or presence of 2-DG is shown in the upper statistical graph (n = 2). DCFDA staining in cells stimulated in media containing glucose versus galactose is depicted in the lower graph (n = 3; **p < 0.01, two-tailed paired t test). Lower left row: cell division versus phosphorylated S6 ribosomal protein in B cells stimulated with LPS for 3 days in the absence or presence of 2-DG (0, 0.25, 0.5, and 1.0 mM left to right) is shown. The graph indicates the frequency of $pS6^{hi}$ B cells in the indicated conditions (n = 3; **p < 0.01 or ***p < 0.005 comparing 2-DG-treated groups to no drug-treated group, repeated-measures one-way ANOVA).
See also Figure S3.

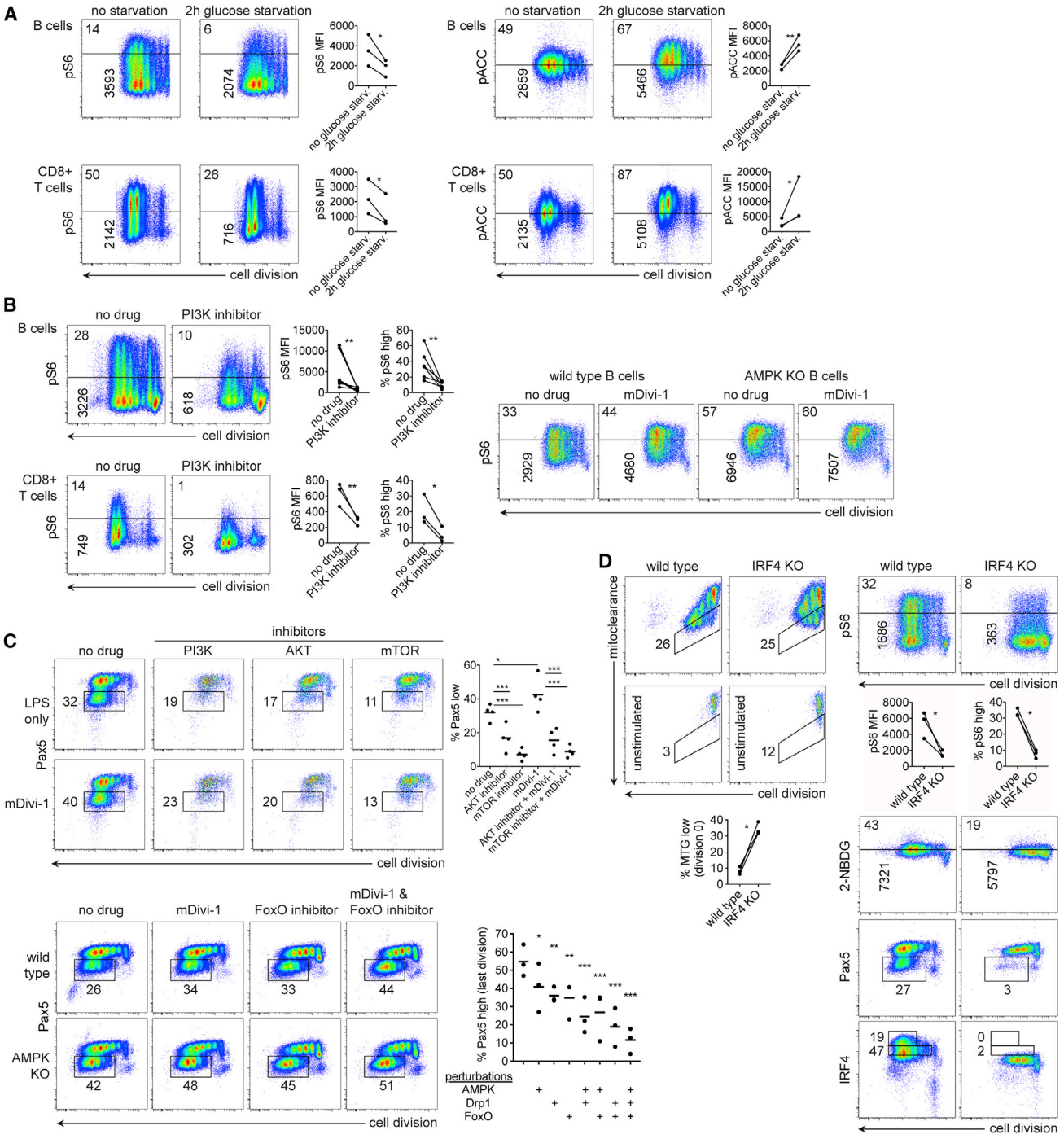

Figure 4. Anabolic-Catabolic Bistability Balancing Differentiation and Renewal

(A) Top panels: cell division versus activation of mTOR (pS6, first two columns) or AMPK (indexed by phospho-Acetyl-CoA Caboxylase, second two columns). Top row: CTV-labeled B cells were stimulated with LPS for 68 hr, without or with glucose starvation for the last 2 hr. Bottom row: CTV-labeled P14 CD8$^+$ T cells were stimulated with gp33-41 peptide and IL-2 for 3 days, without or with glucose starvation for the last 2 hr. Statistics denote MFI of pS6 staining for LPS-activated B cells (upper left) and gp33-41 peptide/APCs/IL-2-activated P14 CD8$^+$ T cells (lower left) and MFI of pACC staining for LPS-activated B cells (upper right) and activated P14 CD8$^+$ T cells (lower right) done after no glucose starvation or 2 hr of glucose starvation (n = 3 for each cell type; *$p < 0.05$ or **$p < 0.01$, two-tailed paired t tests).

(B) Left panels: cell division versus mTOR activation (pS6) in the absence or presence of PI3K inhibitor (5 μM; added 18 hr after stimulation for B cells). CTV-labeled B cells stimulated with LPS (upper row) and CTV-labeled P14 CD8$^+$ T cells stimulated with gp33-41 peptide and IL-2 (lower row) were each analyzed 3 days after stimulation. Statistics are MFI of pS6 (left) frequency of pS6^{hi} cells (right) (n = 3 for each cell type; *$p < 0.05$ or **$p < 0.01$, two-tailed paired t tests). Right panels: B

(legend continued on next page)

(5×10^5 cells per well) were cultured in Iscove's complete media containing human recombinant IL-2 (100 units/mL) in 48-well plates coated with anti-CD3/anti-CD28 antibodies (1 μg/mL; Bio X Cell).

For stimulation of $CD8^+$ T cells from P14 mice, single-cell suspensions from whole spleens were prepared and cultured in Iscove's complete media, unless specified otherwise, containing gp33-41 peptide (1 μg/mL) plus IL-2 (100 units/mL). For glucose deprivation experiments, B cells or P14 $CD8^+$ T cells were cultured in glucose-free/2 mM glutamine-replete RPMI (Gibco) supplemented with fetal calf serum (dialyzed overnight with SnakeSkin dialysis tubing 10K MWCO; Thermo Fisher Scientific) and either 10 mM D-(+)-glucose (Sigma) or 10 mM D-(+)-galactose (Sigma). Compounds used in cell culture included the following: mDivi-1 (Cayman), Chloroquine (Enzo Life Sciences), metformin (AMPK activator; Calbiochem), rapamycin (mTOR inhibitor; Selleckchem), NAC (Sigma), 2-DG (Sigma), LY294002 (PI3K inhibitor; Cell Signaling Technology), Triciribine (AKT inhibitor; Cayman), AS1842856 (FoxO1 inhibitor; Calbiochem), and oligomycin (Sigma).

Retroviral Transduction

Enriched B cells or $CD8^+$ T cells were stimulated with LPS or plate-bound anti-CD3/anti-CD28 antibodies plus IL-2, respectively, for 36 hr prior to retroviral transduction. Cells were then re-plated in supernatant collected prior to transduction. Retroviral constructs used were as follows: mCherry-alpha-tubulin fusion protein (Day et al., 2009); mouse dominant-negative Drp1(K38A), a gift from David Chan (Addgene plasmid 26049) and subsequently cloned into the MSCV-IRES-Thy1.1 plasmid, a gift from Anjana Rao (Addgene plasmid 17442); and hexokinase 2, made by subcloning the rat hexokinase 2 coding sequence into an MSCV-IRES-GFP vector. Empty MSCV-IRES-Thy1.1 or MSCV-IRES-GFP vectors were used as controls.

Organelle Pulse Labeling

Cells were labeled with Cell Trace Violet (CTV; Thermo Fisher Scientific) prior to stimulation to track cell division. Mitochondria were pulse-labeled with MitoTracker Green FM or MitoTracker Red FM (200 nM per 1×10^6 cells) at 37°C for 15 min. Lysosomes were labeled with LysoTracker Deep Red (Thermo Fisher Scientific; 50–75 nM) for 30 min at 37°C in media. Labeling steps were followed by at least two washing steps in cell culture media. For in vivo infections, $Thy1.1^+$ $P14^+$ $CD8^+$ T cells were purified and pulse-labeled with CTV and MitoTracker Green FM and then adoptively transferred into $Thy1.2^+$ recipients that had been infected intravenously 4 hr prior with *Listeria monocytogenes*-expressing LCMV gp33-41 peptide (LMgp33; 5,000 colony-forming units [CFUs]/mouse). Also, 1×10^6 OT-II $Thy1.1^+$ CD4 T cells were purified, pulse-labeled with CTV and MitoTracker Green FM, and then adoptively transferred into Thy1.2+ recipients 24 hr before intranasal infection with 250 50%-tissue culture-infective dose PR8-OVA influenza virus.

Flow Cytometry

Detection of intranuclear antigens was performed using antibodies as previously described (Lin et al., 2015). For detection of phosphorylated antigens, cells were fixed in 4% paraformaldehyde (PFA; Electron Microscopy Sciences) for 15 min, treated with ice-cold methanol (Sigma) for 10 min, and washed twice prior to staining with antibodies (all from Cell Signaling Technology) specific to the following phosphorylated antigens: S6 Ribosomal Protein-S235/236 (clone D57.2.2E conjugated to phycoerythrin (PE); 1:100–400) and Acetyl-CoA Caboxylase (ACC)-S79 (clone D7D11 unconjugated; 1:100). Unconjugated rabbit antibodies (p-ACC) were detected by staining cells with goat anti-rabbit antibodies conjugated to AlexaFluor647 (Thermo Fisher Scientific; 1:1,000). Autophagic organelles were labeled with CYTO-ID Autophagy Detection Kit (Enzo Life Sciences; 1:1,000 dilution of stock) according to the manufacturer's instructions. ROS were detected by incubating cells with MitoSOX Red Mitochondrial Superoxide Indicator (Thermo Fisher Scientific; 5 μM) for 15 min at 37°C in media or CM-H2DCFDA (Thermo Fisher Scientific; 5 μM) for 30 min at 37°C in media. Glucose uptake was measured by incubating cells in 2-NBDG (Cayman; 100 μM) for 45 min at 37°C in glucose-free media. Flow cytometry data were analyzed using FlowJo software (version [v.] 8 and v. 10).

Confocal Microscopy

Confocal microcopy was performed as described (Chang et al., 2011; Lin et al., 2015). Using transmitted light morphology, tubulin bridge staining, and DNA staining, specific identification of telophase or cytokinetic sibling pairs, with the exclusion of any spurious neighboring but unrelated cell pairs, was achieved (Lin et al., 2015). For fixed-cell imaging, cells were adhered to poly-l-lysine- (Sigma) coated coverslips (1.5; Thermo Fisher Scientific) and treated with freshly prepared 3.7% PFA (Sigma) diluted in cell culture media (pH 6.8) in order to preserve mitochondrial morphology and MitoTracker Red FM fluorescence intensity. Following a brief treatment with 0.1% triton, cells were stained with antibody against α-tubulin (clone YOL1/34; Abcam; 1:300) and then anti-rabbit antibody conjugated to AlexaFluor568 (Thermo Fisher Scientific) in a PBS solution containing 0.01% saponin and 0.25% fish skin gelatin (Sigma). For live-cell imaging, cells were transferred to poly-L-lysine-coated eight-chambered coverglass wells (1; LabTek) in warm cell culture media and allowed to adhere briefly before imaging. Images were acquired on inverted confocal microscopes (Zeiss LSM710 or Nikon Ti Eclipse) and processed using ImageJ (v. 1.46r) or Fiji (v. 2.0) software. Total fluorescence in defined regions of single cells was quantitated using the integrated density function in ImageJ.

Statistical Analyses

Significance between experimental groups was determined using two-tailed t tests or two-tailed ratio t tests for paired data, two-tailed Mann-Whitney test for unpaired data, or repeated-measures one-way ANOVA. Two-tailed Fisher's exact test was used to determine significance for contingency statistics of microscopy data comparing asymmetric versus symmetric fluorescence intensity of molecules between sibling pairs. Statistical analyses and summary statistics to determine means and SDs were carried out using GraphPad Prism software v. 7 (*$p < 0.05$, **$p < 0.01$, and ***$p < 0.005$).

SUPPLEMENTAL INFORMATION

Supplemental Information includes four figures and can be found with this article online at http://dx.doi.org/10.1016/j.celrep.2016.11.065.

cells from wild-type and AMPKα1-knockout mice stimulated with LPS for 3 days in the absence or presence of mDivi-1 (10 μM) were analyzed for cell division versus pS6. Data are representative of two identical experiments.

(C) Upper panels: cell division versus Pax5 expression of CTV-labeled B cells stimulated with LPS for 66 hr in the absence or presence of mDivi-1 and inhibitors of PI3K (5 μM), AKT (50 nM), and mTOR (1 nM). Graph contains the frequency of $Pax5^{lo}$ B cells among the indicated groups (n = 4; *$p < 0.05$ or ***$p < 0.005$, repeated-measures one-way ANOVA). Cells activated in the presence of PI3K inhibitor are not included in graph but representative of two identical experiments. Lower panels: cell division versus Pax5 expression of CTV-labeled B cells from wild-type and AMPK-knockout mice stimulated with LPS for 3 days in the absence or presence of mDivi-1 (10 μM), FoxO1 inhibitor (1 μM), or both inhibitors is shown. The graph contains the frequency of $Pax5^{hi}$ cells in the last cell division among the conditions indicated (n = 3; *$p < 0.05$, **$p < 0.01$, or ***$p < 0.005$ comparing groups with one or more perturbations to group with no perturbation, repeated-measures one-way ANOVA).

(D) Left two columns: B cells from wild-type and IRF4-knockout mice left unstimulated (bottom row) or stimulated with LPS for 66 hr (top row) were analyzed for cell division versus mitoclearance. The graph contains MFI of MTG signal in first cell generation of stimulated cells (n = 3; *$p < 0.05$, two-tailed paired t test). Right two columns: CTV-labeled B cells from wild-type and IRF4-knockout mice stimulated with LPS for 66 hr were analyzed for cell division versus pS6, glucose uptake (2-NBDG), Pax5, and IRF4. Statistics denote MFI of pS6 (left) and the frequency of $pS6^{hi}$ cells (right) (n = 3; *$p < 0.05$, two-tailed paired t test). 2-NBDG uptake is representative of two identical experiments. Pax5 and IRF4 staining is repetitive of published findings (Lin et al., 2015).

See also Figure S4.

AUTHOR CONTRIBUTIONS

W.C.A., Y.-H.C., and R.K. planned and performed experiments and wrote the manuscript. B.Y. performed experiments. S.A.N. and W.-H.W.L provided methodologies. N.J.R. provided technical assistance. L.L.L., U.K., M.B., J.C.R., and H.-W.S. provided critical reagents and methodology. S.L.R. supervised and planned experiments and wrote the manuscript.

ACKNOWLEDGMENTS

We are grateful to Benoit Viollet as well as Franck Polleux and Annie Lee for permission to use and provision of AMPKα1-deficient B cells. This work was supported by NIH grants AI061699, AI113365, and AI076458 and the Charles H. Revson Foundation.

Received: July 26, 2016
Revised: October 24, 2016
Accepted: November 21, 2016
Published: December 20, 2016

REFERENCES

Bengsch, B., Johnson, A.L., Kurachi, M., Odorizzi, P.M., Pauken, K.E., Attanasio, J., Stelekati, E., McLane, L.M., Paley, M.A., Delgoffe, G.M., and Wherry, E.J. (2016). Bioenergetic insufficiencies due to metabolic alterations regulated by the inhibitory receptor PD-1 are an early driver of CD8(+) T cell exhaustion. Immunity *45*, 358–373.

Buck, M.D., O'Sullivan, D., Klein Geltink, R.I., Curtis, J.D., Chang, C.H., Sanin, D.E., Qiu, J., Kretz, O., Braas, D., van der Windt, G.J., et al. (2016). Mitochondrial dynamics controls T cell fate through metabolic Programming. Cell *166*, 63–76.

Caro-Maldonado, A., Wang, R., Nichols, A.G., Kuraoka, M., Milasta, S., Sun, L.D., Gavin, A.L., Abel, E.D., Kelsoe, G., Green, D.R., and Rathmell, J.C. (2014). Metabolic reprogramming is required for antibody production that is suppressed in anergic but exaggerated in chronically BAFF-exposed B cells. J. Immunol. *192*, 3626–3636.

Chang, J.T., Ciocca, M.L., Kinjyo, I., Palanivel, V.R., McClurkin, C.E., Dejong, C.S., Mooney, E.C., Kim, J.S., Steinel, N.C., Oliaro, J., et al. (2011). Asymmetric proteasome segregation as a mechanism for unequal partitioning of the transcription factor T-bet during T lymphocyte division. Immunity *34*, 492–504.

Chang, C.H., Curtis, J.D., Maggi, L.B., Jr., Faubert, B., Villarino, A.V., O'Sullivan, D., Huang, S.C., van der Windt, G.J., Blagih, J., Qiu, J., et al. (2013). Posttranscriptional control of T cell effector function by aerobic glycolysis. Cell *153*, 1239–1251.

Chazotte, B. (2011). Labeling mitochondria with MitoTracker dyes. Cold Spring Harb. Protoc. *2011*, 990–992.

Day, D., Pham, K., Ludford-Menting, M.J., Oliaro, J., Izon, D., Russell, S.M., and Gu, M. (2009). A method for prolonged imaging of motile lymphocytes. Immunol. Cell Biol. *87*, 154–158.

Frank, S., Gaume, B., Bergmann-Leitner, E.S., Leitner, W.W., Robert, E.G., Catez, F., Smith, C.L., and Youle, R.J. (2001). The role of dynamin-related protein 1, a mediator of mitochondrial fission, in apoptosis. Dev. Cell *1*, 515–525.

Frauwirth, K.A., Riley, J.L., Harris, M.H., Parry, R.V., Rathmell, J.C., Plas, D.R., Elstrom, R.L., June, C.H., and Thompson, C.B. (2002). The CD28 signaling pathway regulates glucose metabolism. Immunity *16*, 769–777.

Fuxa, M., and Busslinger, M. (2007). Reporter gene insertions reveal a strictly B lymphoid-specific expression pattern of Pax5 in support of its B cell identity function. J. Immunol. *178*, 3031–3037.

García-Prat, L., Martínez-Vicente, M., Perdiguero, E., Ortet, L., Rodríguez-Ubreva, J., Rebollo, E., Ruiz-Bonilla, V., Gutarra, S., Ballestar, E., Serrano, A.L., et al. (2016). Autophagy maintains stemness by preventing senescence. Nature *529*, 37–42.

Im, S.J., Hashimoto, M., Gerner, M.Y., Lee, J., Kissick, H.T., Burger, M.C., Shan, Q., Hale, J.S., Lee, J., Nasti, T.H., et al. (2016). Defining CD8(+) T cells that provide the proliferative burst after PD-1 therapy. Nature *537*, 417–421.

Iritani, B.M., and Eisenman, R.N. (1999). c-Myc enhances protein synthesis and cell size during B lymphocyte development. Proc. Natl. Acad. Sci. USA *96*, 13180–13185.

Ito, K., Turcotte, R., Cui, J., Zimmerman, S.E., Pinho, S., Mizoguchi, T., Arai, F., Runnels, J.M., Alt, C., Teruya-Feldstein, J., et al. (2016). Self-renewal of a purified Tie2+ hematopoietic stem cell population relies on mitochondrial clearance. Science, aaf5530. http://dx.doi.org/10.1126/science.aaf5530.

Jørgensen, S.B., Viollet, B., Andreelli, F., Frøsig, C., Birk, J.B., Schjerling, P., Vaulont, S., Richter, E.A., and Wojtaszewski, J.F. (2004). Knockout of the alpha2 but not alpha1 5′-AMP-activated protein kinase isoform abolishes 5-aminoimidazole-4-carboxamide-1-beta-4-ribofuranosidebut not contraction-induced glucose uptake in skeletal muscle. J. Biol. Chem. *279*, 1070–1079.

Katajisto, P., Döhla, J., Chaffer, C.L., Pentinmikko, N., Marjanovic, N., Iqbal, S., Zoncu, R., Chen, W., Weinberg, R.A., and Sabatini, D.M. (2015). Stem cells. Asymmetric apportioning of aged mitochondria between daughter cells is required for stemness. Science *348*, 340–343.

Keppler, S.J., Gasparrini, F., Burbage, M., Aggarwal, S., Frederico, B., Geha, R.S., Way, M., Bruckbauer, A., and Batista, F.D. (2015). Wiskott-Aldrich syndrome interacting protein deficiency uncovers the role of the co-receptor CD19 as a generic hub for PI3 kinase signaling in B cells. Immunity *43*, 660–673.

Khacho, M., Clark, A., Svoboda, D.S., Azzi, J., MacLaurin, J.G., Meghaizel, C., Sesaki, H., Lagace, D.C., Germain, M., Harper, M.E., et al. (2016). Mitochondrial dynamics impacts stem cell identity and fate decisions by regulating a nuclear transcriptional program. Cell Stem Cell *19*, 232–247.

Klein, U., Casola, S., Cattoretti, G., Shen, Q., Lia, M., Mo, T., Ludwig, T., Rajewsky, K., and Dalla-Favera, R. (2006). Transcription factor IRF4 controls plasma cell differentiation and class-switch recombination. Nat. Immunol. *7*, 773–782.

Lin, W.H., Adams, W.C., Nish, S.A., Chen, Y.H., Yen, B., Rothman, N.J., Kratchmarov, R., Okada, T., Klein, U., and Reiner, S.L. (2015). Asymmetric PI3K signaling driving developmental and regenerative cell fate bifurcation. Cell Rep. *13*, 2203–2218.

Lin, W.W., Nish, S.A., Yen, B., Chen, Y.H., Adams, W.C., Kratchmarov, R., Rothman, N.J., Bhandoola, A., Xue, H.H., and Reiner, S.L. (2016). CD8+ T lymphocyte self-renewal during effector cell determination. Cell Rep. *17*, 1773–1782.

Luchsinger, L.L., de Almeida, M.J., Corrigan, D.J., Mumau, M., and Snoeck, H.W. (2016). Mitofusin 2 maintains haematopoietic stem cells with extensive lymphoid potential. Nature *529*, 528–531.

Man, K., Miasari, M., Shi, W., Xin, A., Henstridge, D.C., Preston, S., Pellegrini, M., Belz, G.T., Smyth, G.K., Febbraio, M.A., et al. (2013). The transcription factor IRF4 is essential for TCR affinity-mediated metabolic programming and clonal expansion of T cells. Nat. Immunol. *14*, 1155–1165.

Mishra, P., and Chan, D.C. (2014). Mitochondrial dynamics and inheritance during cell division, development and disease. Nat. Rev. Mol. Cell Biol. *15*, 634–646.

Nish, S.A., Zens, K.D., Kratchmarov, R., Lin, W.H., Adams, W.C., Chen, Y.H., Yen, B., Rothman, N.J., Bhandoola, A., Xue, H.H., et al. (2017). CD4+ T cell effector commitment coupled to self-renewal by asymmetric cell divisions. J. Exp. Med. http://dx.doi.org/10.1084/jem.20161046

O'Sullivan, T.E., Johnson, L.R., Kang, H.H., and Sun, J.C. (2015). BNIP3- and BNIP3L-mediated mitophagy promotes the generation of natural killer cell memory. Immunity *43*, 331–342.

Quah, B.J., and Parish, C.R. (2012). New and improved methods for measuring lymphocyte proliferation in vitro and in vivo using CFSE-like fluorescent dyes. J. Immunol. Methods *379*, 1–14.

Rathmell, J.C., Vander Heiden, M.G., Harris, M.H., Frauwirth, K.A., and Thompson, C.B. (2000). In the absence of extrinsic signals, nutrient utilization

by lymphocytes is insufficient to maintain either cell size or viability. Mol. Cell *6*, 683–692.

Roberts, D.J., and Miyamoto, S. (2015). Hexokinase II integrates energy metabolism and cellular protection: Akting on mitochondria and TORCing to autophagy. Cell Death Differ. *22*, 248–257.

Rolf, J., Zarrouk, M., Finlay, D.K., Foretz, M., Viollet, B., and Cantrell, D.A. (2013). AMPKα1: a glucose sensor that controls CD8 T-cell memory. Eur. J. Immunol. *43*, 889–896.

Scharping, N.E., Menk, A.V., Moreci, R.S., Whetstone, R.D., Dadey, R.E., Watkins, S.C., Ferris, R.L., and Delgoffe, G.M. (2016). The tumor microenvironment represses T cell mitochondrial biogenesis to drive intratumoral T cell metabolic insufficiency and dysfunction. Immunity *45*, 374–388.

Shi, W., Liao, Y., Willis, S.N., Taubenheim, N., Inouye, M., Tarlinton, D.M., Smyth, G.K., Hodgkin, P.D., Nutt, S.L., and Corcoran, L.M. (2015). Transcriptional profiling of mouse B cell terminal differentiation defines a signature for antibody-secreting plasma cells. Nat. Immunol. *16*, 663–673.

Sukumar, M., Liu, J., Ji, Y., Subramanian, M., Crompton, J.G., Yu, Z., Roychoudhuri, R., Palmer, D.C., Muranski, P., Karoly, E.D., et al. (2013). Inhibiting glycolytic metabolism enhances CD8+ T cell memory and antitumor function. J. Clin. Invest. *123*, 4479–4488.

Utzschneider, D.T., Charmoy, M., Chennupati, V., Pousse, L., Ferreira, D.P., Calderon-Copete, S., Danilo, M., Alfei, F., Hofmann, M., Wieland, D., et al. (2016). T cell factor 1-expressing memory-like CD8(+) T cells sustain the immune response to chronic viral infections. Immunity *45*, 415–427.

Xu, H., Chaudhri, V.K., Wu, Z., Biliouris, K., Dienger-Stambaugh, K., Rochman, Y., and Singh, H. (2015). Regulation of bifurcating B cell trajectories by mutual antagonism between transcription factors IRF4 and IRF8. Nat. Immunol. *16*, 1274–1281.